Analysis and Calculation of DC-Link Current and Voltage Ripples for Three-Phase Inverter With Unbalanced Load

Xuejun Pei, *Member, IEEE*, Wu Zhou, and Yong Kang

***Abstract*—In this paper, an analysis and calculation of the dc-link current and voltage ripples are presented for a three-phase inverter with unbalanced load. A comparison of the dc-link average and root-mean-square (rms) currents between considering and ignoring high frequency harmonics of the output current is drawn. It is shown that high frequency harmonic currents have little effect on the dc-link current, and therefore, they can be ignored. Based on the symmetrical components method, the dc-link average and harmonic rms currents are derived, and the dc-link voltage ripple is compared between the balanced and unbalanced loads. It can be found that the dc-link current and voltage ripples consist of not only high frequency harmonics but also the double fundamental frequency harmonic, and the voltage ripple is independent of the positive-sequence component and determined by the negative-sequence component, under the unbalanced load. Experimental results are shown to verify the accuracy of the theoretical analysis.**

***Index Terms*—DC-link current, double fundamental frequency harmonic, symmetrical components method, unbalanced load.**

I. Introduction

With the development of industry, the need for a three-phase inverter to improve power quality is rapidly growing in many high-power applications, such as uninterruptible power supply (UPS), motor drive, flexible ac transmission, and renewable energy generation. In order to control output voltages of the three-phase inverter as a sinusoidal waveform, pulse width modulation (PWM) is commonly used, even with an unbalanced load. The PWM technique pushes harmonics into high frequency range, that is, the switching frequency f_c and its multiples $2f_c$, $3f_c$, and so on. As a result, the purely sinusoidal output voltages are obtained when an output filter is utilized. Some PWM techniques for the inverter have been proposed to achieve the sinusoidal output voltages and improve other performances [1]–[4]. The double Fourier series analytical method is commonly used to determine output harmonics generated by the PWM process [5]. Meanwhile, the dc-link current of the inverter includes a dc component and harmonics with the PWM strategy. The dc component comes from the dc source, and however, most of the harmonics should be attenuated by an input filter, resulting in few harmonics flowing through the dc source. A dc-link capacitor and an inductor (including the stray and external inductor) constitute the input filter to deal with the harmonics of the dc-link current [6]. Since the dc-link capacitor contributes substantially to the volume, weight, and cost, an overdesign of the dc-link capacitor should be avoided. On the other hand, if the dc-link capacitance is too small, the high dc-link voltage ripple appears and influences the PWM process. Ultimately, it may cause the distortion of the output voltages, although the feedback control is utilized. Therefore, the analysis of the dc-link current and voltage ripples is essential for the dc-link capacitor design [7]–[10].

Some researchers have concentrated on the analysis of the dc-link current and voltage ripples with the Fourier series and root-mean-square (rms) calculation for the balanced load [11]–[18]. In [11], a general expression for the spectrum of the dc-link current was introduced by using the Fourier series of switching functions for the single- and three-phase inverter. Holmes *et al.* presented a generalized analytical approach, in which the product of the switching functions and the load currents was evaluated in the frequency domain based on the convolution calculation [12]. In [13]–[15], dc-link current harmonics were analyzed for the single- and three-phase voltage-source inverter and converter based on the double Fourier series. Although spectrum results of the Fourier transformation are intuitive, the calculation of the inverter switching functions is difficult and requires much computer memory. In [16] and [17], the analysis and minimization of the harmonic components of the dc-link current and voltage were presented based on the calculation of the rms value of the dc-link current and voltage. The calculation result shows a simple expression for the balanced load, regardless of different modulation patterns. However, the formulation of the dc-link voltage ripple is too complex for the dc-link capacitor design. In [18], a new PWM strategy was presented to reduce the dc-link current ripple. Nevertheless, the PWM modulation method is rarely used in the practical application. In the aforementioned majority of literatures, the balanced load is assumed for the dc-link current analytical calculation. In [19], based on the power balance principle of dc input and ac output sides, a dc-link current calculating method was proposed under the unbalanced and nonlinear loads. However, the modulation pattern is out of consideration, and the dc-link voltage is as-

Manuscript received August 25, 2014; revised October 24, 2014; accepted November 17, 2014. Date of publication December 2, 2014; date of current version May 22, 2015. This work was supported by Grants from the Power Electronics Science and Education Development Program of Delta Environmental & Educational Foundation (DREK 2013001). Recommended for publication by Associate Editor Dr. A. M. Trzynadlowski.

The authors are with the State Key Laboratory of Advanced Electromagnetic Engineering and Technology, Huazhong University of Science and Technology, Wuhan 430074, China (e-mail: ppei215@mail.hust.edu.cn; zhouwu@hust.edu.cn; ykang@mail.hust.edu.cn).

Color versions of one or more of the figures in this paper are available online at http://ieeexplore.ieee.org.

Digital Object Identifier 10.1109/TPEL.2014.2375353

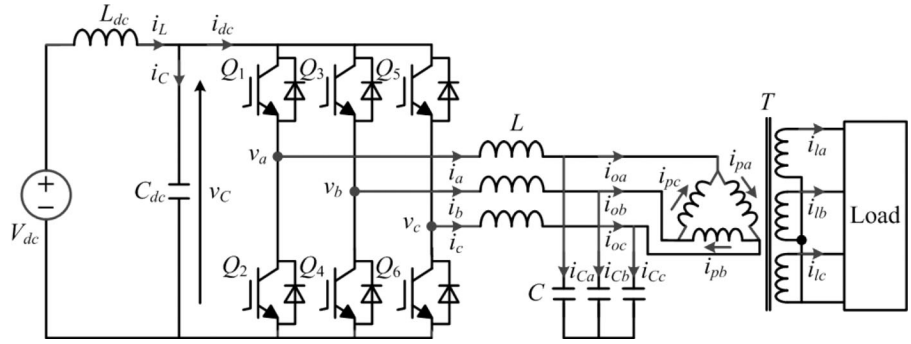

Fig. 1. Topology of the three-phase bridge inverter.

sumed constant. Until now, little work has been done for the dc-link voltage ripple, which is also important for the dc-link capacitor design.

This paper presents the analysis and calculation of the dc-link current and voltage ripples for the three-phase inverter with the unbalanced load. It is found that high frequency harmonics of the output currents have little effect on the dc-link current, and therefore, they can be ignored. Applying the symmetrical components method, the dc-link average and harmonic rms currents are derived, and the dc-link voltage ripple is obtained under the balanced and unbalanced loads. It can be found that the voltage ripple under the unbalanced load is independent of the positive-sequence component and determined by the negative-sequence component. As a result, the dc-link capacitor design can be simplified.

This paper is organized as follows. In Section II, the system configuration and reference signal are introduced. Section III analyzes the effect of high frequency harmonic currents on the dc-link current. The dc-link average and harmonic rms currents are derived in Section IV, followed by the calculation of the dc-link voltage ripple in Section V. Experimental results are presented in Section VI. Finally, a conclusion is drawn in Section VII.

II. System Configuration and Reference Signal

A. System Configuration

Fig. 1 shows the topology of the three-phase bridge inverter. It is assumed that the inverter is supplied by a constant ripple-free dc voltage source $V_{\rm dc}$. $Q_1 \sim Q_6$ are IGBT switching devices, which are controlled by the digital signal processor (DSP) with isolated gate drivers. $C_{\rm dc}$ is the dc-link capacitor, and $L_{\rm dc}$ is the dc-link inductor from the dc source to $C_{\rm dc}$, including the parasitic inductor. *L* and *C* form a second-order output filter to attenuate high frequency harmonics. A power transformer (*T*) is inserted between the output filter (*LC*) and the load to achieve the galvanic isolation and provide a grounded neutral terminal in the Y-connected secondary windings, which can be used to carry the unbalanced load currents. The primary windings are usually Δ-connected because the undesirable third-harmonic currents are trapped inside the Δ-connected windings.

From the standpoint of the dc-link, the inverter bridge, filter, and load can be equal to the dc-link current $i_{\rm dc}$, which is made up of the dc current and harmonic components. In this case, the equivalent circuit is shown in Fig. 2. Because the impedance of the dc-link capacitor is infinity for the dc current, the dc current only flows through the dc-link inductor and absorbs the active power from the dc source. Moreover, due to the dc-link capacitor, the dc-link voltage is approximately kept constant. $C_{\rm dc}$ and $L_{\rm dc}$ (including the stray and external inductor) constitute the dc-link filter, which is used to attenuate harmonic components of the dc-link current.

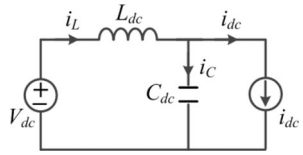

Fig. 2. Equivalent circuit of dc-link.

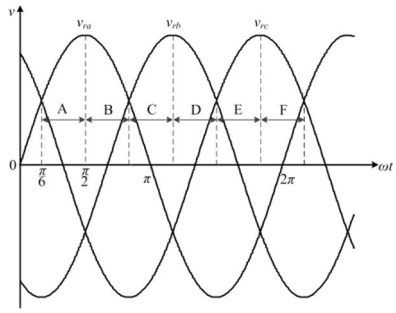

Fig. 3. Three-phase reference signals.

The status of any switch can be represented by the switching functions S_{Q1}, S_{Q2}, and so on. The switching function is binary: the switching function is 1 when the switch is turned ON, and the switching function is 0 when the switch is turned OFF. Neglecting the dead time, the gating signals of the upper and lower switches in the same arm are complementary. For a bridge arm, the dc-link current is equal to the corresponding output current when the upper switch is turned ON, and the dc-link current is zero when the upper switch is turned OFF. The dc-link current $i_{\rm dc}$ is the sum of three bridge arm currents. Consequently, the dc-link current can be expressed as

$$i_{\rm dc} = S_{Q1} i_a + S_{Q3} i_b + S_{Q5} i_c \tag{1}$$

where S_{Q1}, S_{Q3}, and S_{Q5} are the switching functions of Q_1, Q_3, and Q_5, respectively. i_a, i_b, and i_c are the three-phase output

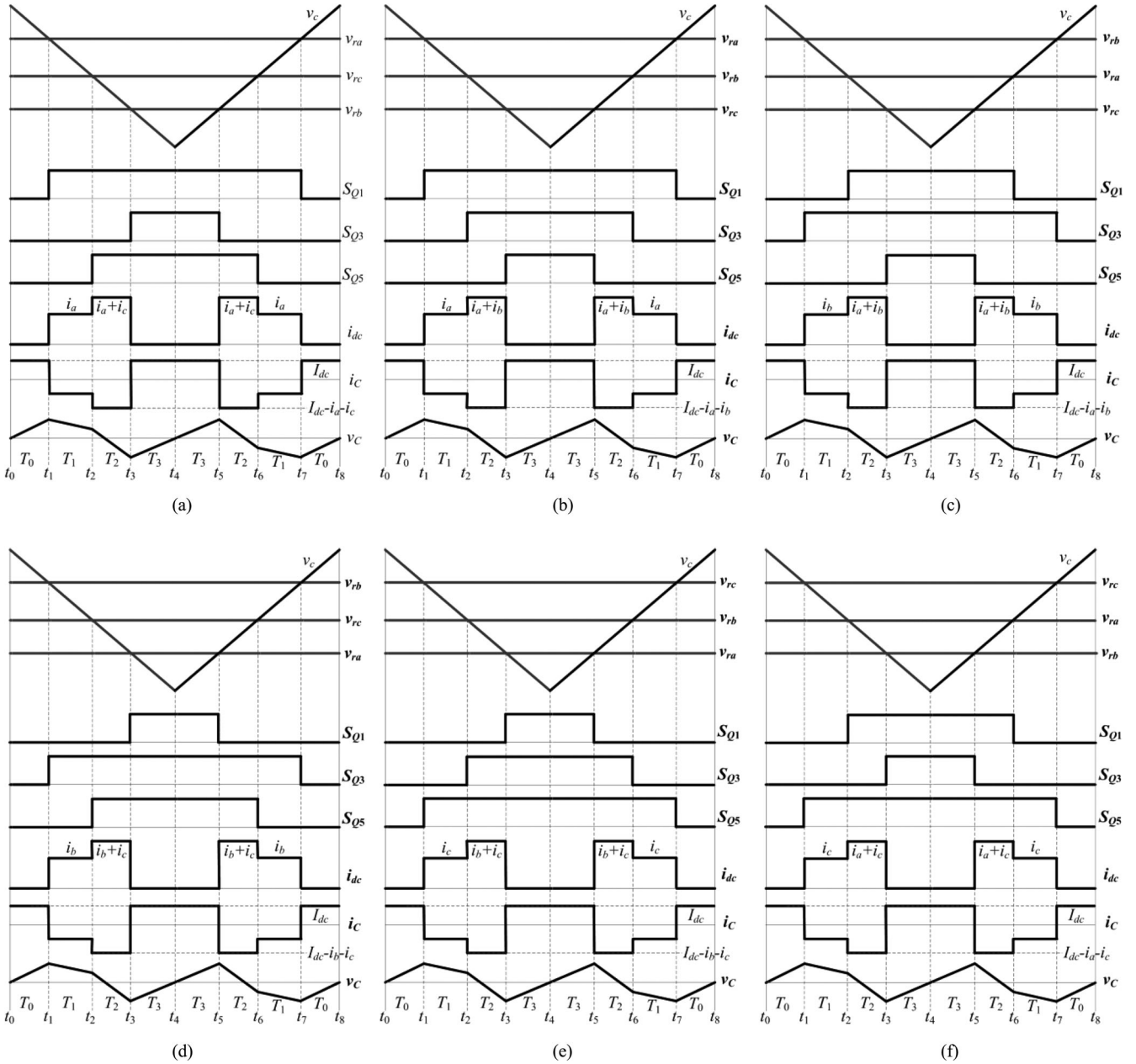

Fig. 4. Detailed PWM signals over six intervals: (a) Interval A, (b) Interval B, (c) Interval C, (d) Interval D, (e) Interval E, and (f) Interval F.

currents of the inverter bridge. One can note that the ripple of $i_{\rm dc}$ is high because of the frequent jumps between the output currents and zero.

B. Reference Signal

In the three-phase inverter, the commonly used PWM technique is sinusoidal pulse width modulation (SPWM), third-harmonic PWM, and space vector modulation (SVM). The third-harmonic PWM is that the reference signal consists of a fundamental component and a third-harmonic component. In contrast to the sinusoidal and third-harmonic PWM, SVM does not consider each of the three modulating voltages as a separate identity. However, in fact, SVM is also similar to the harmonic injection method. Therefore, the general three-phase reference signals can be expressed as

$$\begin{cases} v_{ra} = MV_{cm}[\sin(\omega t) + v_z] \\ v_{rb} = MV_{cm}[\sin(\omega t - 120^o) + v_z] \\ v_{rc} = MV_{cm}[\sin(\omega t + 120^o) + v_z] \end{cases} \tag{2}$$

where ω is the fundamental angular frequency of the output voltages, V_{cm} is the magnitude of the reference signals, *M* is the modulation index, and v_z is the signal, which is injected into the three reference signals. The injected signals are defined as follows.

1) For SPWM, $v_z = 0$.

2) For the third-harmonic PWM, v_z can be written as

$$v_z = \frac{1}{6}\sin 3\,\omega t. \tag{3}$$

3) For SVM, the injected signal is

$$v_z = -\frac{1}{2}(v_{\max} + v_{\min}) \tag{4}$$

where $v_{\max} = \max[\sin\omega t,\ \sin(\omega t - 120^\circ),\ \sin(\omega t + 120^\circ)]$, $v_{\min} = \min[\sin\omega t, \sin(\omega t - 120^\circ), \sin(\omega t + 120^\circ)]$.

Comparing the bidirectional carrier signal v_{cr} with the three reference signals v_{ra}, v_{rb}, and v_{rc} shown in Fig. 3 produces the gating signals of $Q_1 - Q_6$.

From Fig. 3, it can be seen that one fundamental period can be divided into six intervals A–F. Fig. 4 shows the six detailed PWM waveforms over one carrier period during the intervals A–F. Note that when the switching frequency is high enough, the value of the reference signals during one carrier period can be assumed constant. Taking the interval A as an example, according to the modulation waveforms, T_0, T_1, T_2, and T_3 can be solved as

$$\begin{cases} T_0 = \dfrac{T_S}{4}(1 - M\sin\omega t - Mv_z) \\ T_1 = \dfrac{T_S}{4}M[\sin\omega t - \sin(\omega t + 120^\circ)] \\ T_2 = \dfrac{T_S}{4}M[\sin(\omega t + 120^\circ) - \sin(\omega t - 120^\circ)] \\ T_3 = \dfrac{T_S}{4}[1 + M\sin(\omega t - 120^\circ) + Mv_z]. \end{cases} \tag{5}$$

III. Effect of High Frequency Harmonic Currents on DC-Link Current

A. Switching Functions and Output Currents

According to (1), the dc-link current is the product of three switching functions and three corresponding output currents. The switching functions are first taken into consideration. It is widely accepted that harmonics generated by almost any PWM process can be determined by using the double Fourier series [5]. Here, taking the symmetrical sampled SPWM as an example, the double Fourier transformation result can be expressed as

$$\begin{aligned} s_x = {} & \frac{1}{2} + \frac{2}{\pi}\sum_{n=1}^{\infty} \frac{J_n\left(n\frac{\omega_o}{\omega_c}\frac{\pi}{2}M\right)}{n\frac{\omega_o}{\omega_c}} \sin\left(n\left[1 + \frac{\omega_o}{\omega_c}\right]\frac{\pi}{2}\right) \\ & \times \cos\left(n\left[\omega_o t + \theta_{ox} - \frac{\pi}{2}\right]\right) \\ & + \sum_{m=1}^{\infty}\sum_{n=-\infty}^{\infty}\left[\frac{2}{[m + n\omega_o/\omega_c]\,\pi}\right. \\ & \left.\sin\left(\left[m + n\frac{\omega_o}{\omega_c} + n\right]\frac{\pi}{2}\right) J_n\left(\left[m + n\frac{\omega_o}{\omega_c}\right]\frac{\pi}{2}M\right)\right. \\ & \left.\times \cos\left(m\left[\omega_c t - \frac{\pi}{2}\right] + n\left[\omega_o t + \theta_{ox} - \frac{\pi}{2}\right]\right)\right] \end{aligned} \tag{6}$$

where $J_n(\xi)$ denotes a Bessel function of the first kind, with the order n, argument ξ, and fundamental phase angle θ_{ox}, $x \in \{a, b, c\}$. Fig. 5 shows the nominalized spectrum of S_x, when the symmetrical sampled SPWM is utilized and the modulation ratio M is 1. The reference value is that at the fundamental frequency. Obviously, the amplitudes at the carrier frequency and its multiples are attenuated significantly when the order rises. Moreover, baseband harmonics appear near the carrier frequency and its multiples, and they are attenuated significantly with the order, too.

The output currents are generated by the output voltages across the output impedance. Taking the negative terminal of the dc input as the reference point, the output phase voltages can be written as

$$\begin{bmatrix} v_a & v_b & v_c \end{bmatrix}^T = V_{\rm dc}\begin{bmatrix} S_{Q1} & S_{Q3} & S_{Q5} \end{bmatrix}^T. \tag{7}$$

The output currents are given by

$$\begin{aligned} \begin{bmatrix} i_a \\ i_b \\ i_c \end{bmatrix} &= \frac{1}{3Z}\begin{bmatrix} 2 & -1 & -1 \\ -1 & 2 & -1 \\ -1 & -1 & 2 \end{bmatrix}\begin{bmatrix} v_a \\ v_b \\ v_c \end{bmatrix} \\ &= \frac{V_{\rm dc}}{3Z}\begin{bmatrix} 2 & -1 & -1 \\ -1 & 2 & -1 \\ -1 & -1 & 2 \end{bmatrix}\begin{bmatrix} S_{Q1} \\ S_{Q3} \\ S_{Q5} \end{bmatrix} \end{aligned} \tag{8}$$

where Z is the combined impedance of the LC filter and the three-phase Y-connected load. Therefore, the output currents are composed of the load currents and the filter currents. For the unbalanced load, the calculation matrix of the output currents can be obtained by the superimposition principle. The definition of the imbalance is based on the difference between the maximum phase load and the minimum phase load [20]. Based on the definition and requirement, the worst case is one/two phases with full load and other phases with half load. The percentage of the unbalanced load is 50%.

Assuming the load is linear and the load voltages are sinusoidal, because the LC Filter is usually designed to attenuate high frequency output harmonics. For the fundamental frequency, the filter inductor voltages produced by the load currents are much smaller than the output voltages, and thus, the filter inductors can be omitted to analyze the dc-link current. Therefore, a simplified circuit of the ac side for the inverter is shown in Fig. 6(a), in which the load is equal to three sinusoidal current sources i_{la}, i_{lb}, and i_{lc}.

From Fig. 6(a), it can be seen that the filter currents are generated by the output voltages through the LC filter. Since the output voltages consist of the fundamental voltage and high frequency harmonics, the filter currents are made up of the passive fundamental current and high frequency harmonics. Similar to the aforementioned analysis, the filter inductor can be omitted for the passive fundamental current, and thus, the passive fundamental current is mainly determined by the filter capacitor. If

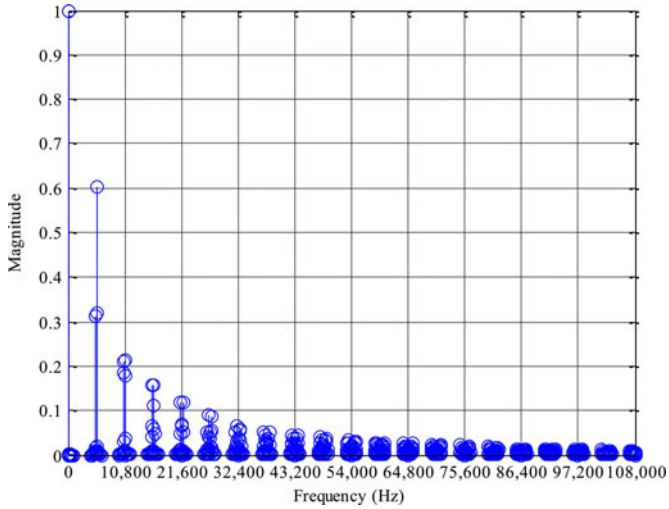

Fig. 5. Nominalized spectrum of S_x when $M = 1$.

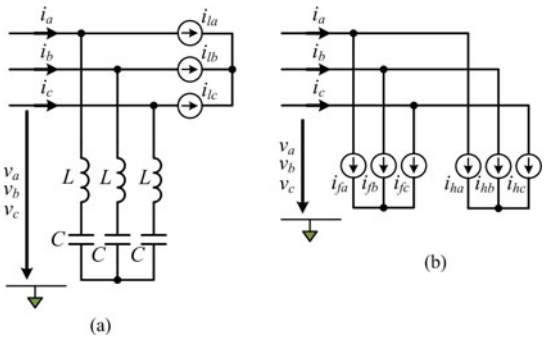

Fig. 6. Simplified circuit of the ac side for three-phase inverter (a) Only considering load currents (b) Considering output currents.

the load currents and the passive fundamental current are combined, the output currents is divided into three fundamental sinusoidal current sources i_{fa}, i_{fb}, and i_{fc}, and three high frequency harmonic currents i_{ha}, i_{hb}, and i_{hc}. As a result, a further simplified equivalent circuit shown in Fig. 6(b) is obtained.

B. Effect of High Frequency Harmonic Currents

To analyze the effect of high frequency harmonic currents on the dc-link current, a comparison of the dc-link average and rms currents between considering and ignoring the high frequency harmonic currents is drawn under the balanced and unbalanced loads. The average and rms currents are defined, respectively, as

$$I_{\rm dc} = \frac{1}{2\pi}\int_0^{2\pi} i_{\rm dc} d\omega t \tag{9}$$

$$I_{rms} = \sqrt{\frac{1}{2\pi}\int_0^{2\pi} i_{\rm dc}^2 d\omega t}. \tag{10}$$

From (1), it can be seen that the dc-link current is the product of three switching functions and three corresponding output currents. Because the direct mathematic expressions of the average and rms currents are too complex to find when considering high frequency harmonic currents, an approximation should be made. From (6) and (8), it is shown that the switching functions and the output currents have similar spectral characteristics. Since both the switching functions and the output currents (or high frequency harmonic currents) are infinite series, they are approximated to finite ones to simplify the calculation. Because of the fast attenuation of multiple carrier frequency and baseband spectra, both the maximum carrier order and baseband are 20th.

Fig. 7 illustrates the comparison results of the dc-link average and rms currents as a function of the modulation index between considering and ignoring high frequency harmonic currents under the balanced and unbalanced loads, when the symmetrical sampled SPWM is used. The *m*-file in MATLAB software is applied to calculate the dc-link current. Inverter specifications and key parameters are shown in Section VI. From Fig. 7(a) and (b), it can be seen that the dc-link average and rms currents between considering and ignoring high frequency harmonic currents have little difference, regardless of the load conditions. It means that high frequency harmonic currents have little influence on the dc-link average and rms currents, and ignoring high frequency harmonic currents is feasible to analyze the dc-link current.

Although the comparison is based on the SPWM modulation, the same comparison results can be obtained for other modulation patterns and are not shown here. As a result, the effect of high frequency harmonic currents is ignored in later Section, and the output currents are supposed to be sinusoidal when analyzing the dc-link current.

IV. DC-Link Average and Harmonic RMS Current

According to the analysis in Section III, the effect of high frequency harmonic currents on the dc-link current can be ignored. Assuming that the load is linear, the general three-phase output currents can be written as

$$\begin{cases} i_a = I_{a\max}\sin(\omega t - \varphi_a) \\ i_b = I_{b\max}\sin(\omega t - \varphi_b - 120^\circ) \\ i_c = I_{c\max}\sin(\omega t - \varphi_c + 120^\circ) \end{cases} \tag{11}$$

where $I_{a\max}$, $I_{b\max}$, and $I_{c\max}$ are the peak values of i_a, i_b, and i_c, respectively. φ_a, φ_b, and φ_c are the phase differences between the phase voltages and currents.

In accordance with the symmetrical components method, the three-phase output currents can be resolved into three sets of symmetrical components: positive-sequence, negative-sequence, and zero-sequence. As a result, the general three-phase output currents can be separated into three balanced and uncoupled networks. When the load is balanced, the output currents have no zero-sequence and negative-sequence components. Assuming that I_a, I_b, and I_c are vectors of i_a, i_b, and i_c and taking phase a as an example, the transformation is defined as

$$\begin{bmatrix} I_a \\ I_b \\ I_c \end{bmatrix} = \begin{bmatrix} 1 & 1 & 1 \\ 1 & a^2 & a \\ 1 & a & a^2 \end{bmatrix} \begin{bmatrix} I_{a0} \\ I_{a1} \\ I_{a2} \end{bmatrix} \tag{12}$$

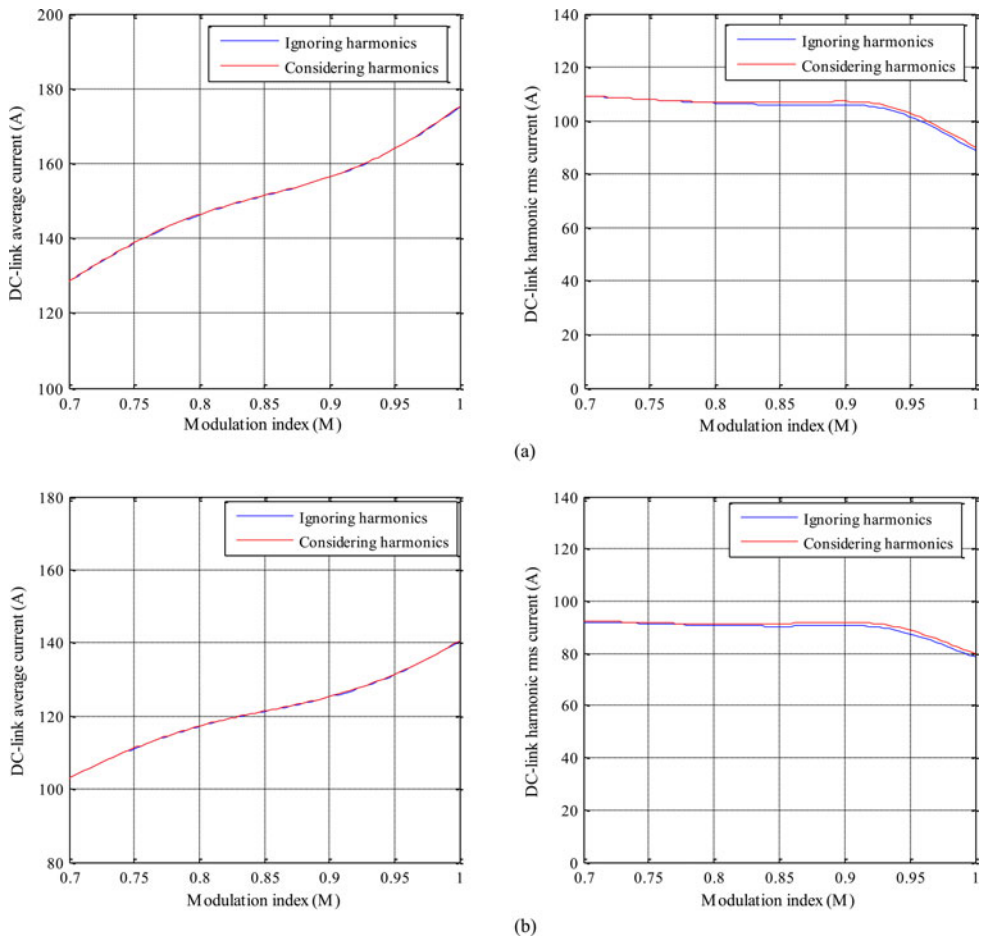

Fig. 7. Comparison results under (a) balanced load, (b) unbalanced load.

where I_{a0}, I_{a1}, and I_{a2} represent the zero, positive, and negative-sequence components of phase a, respectively. a is the complex transformation number $e^{j(2/3)\pi}$. The inverse transformation of (12) is

$$\begin{bmatrix} I_{a0} \\ I_{a1} \\ I_{a2} \end{bmatrix} = \frac{1}{3} \begin{bmatrix} 1 & 1 & 1 \\ 1 & a & a^2 \\ 1 & a^2 & a \end{bmatrix} \begin{bmatrix} I_a \\ I_b \\ I_c \end{bmatrix}. \tag{13}$$

Note that the aforementioned transformation is based on the vector, which is not the transient values of i_a, i_b, and i_c. According to the KCL law, the sum of three phase currents is zero ($I_a + I_b + I_c = 0$), and therefore, the system has no zero-sequence component, which means that I_{a0} is zero. Therefore, only the positive- and negative-sequence components exist under the unbalanced load. The peak values and phase angles of the positive- and negative-sequence components, that is, I_+ and I_-, ϕ and θ, can be calculated based on the vector calculation (see the appendix). It should be noted that the filter capacitor currents should be included in the calculation of I_+ and I_-, ϕ and θ. Consequently, the three-phase output currents can be resolved as

$$\begin{cases} i_a = I_+ \sin(\omega t - \phi) + I_- \sin(\omega t - \theta) \\ i_b = I_+ \sin(\omega t - \phi - 120^\circ) + I_- \sin(\omega t - \theta + 120^\circ) \\ i_c = I_+ \sin(\omega t - \phi + 120^\circ) + I_- \sin(\omega t - \theta - 120^\circ). \end{cases} \tag{14}$$

A. DC-Link Average Current

Since the dc-link average current is the integral of the dc-link current in the whole fundamental period, it is needed to calculate the average current over each interval. From Fig. 4(a), the instant dc-link current $i_{\rm dc}$ in the interval A can be obtained as

$$i_{\rm dc} = \begin{cases} 0 & t_0 \le t \le t_1 \\ i_a & t_1 \le t \le t_2 \\ i_a + i_c & t_2 \le t \le t_3 \\ 0 & t_3 \le t \le t_5 \\ i_a + i_c & t_5 \le t \le t_6 \\ i_a & t_6 \le t \le t_7 \\ 0 & t_7 \le t \le t_8. \end{cases} \tag{15}$$

According to (15), the dc-link average current over one carrier period in the interval A can be calculated as

$$I_{\mathrm{dc}A} = \frac{1}{T_S}\int_{t_0}^{t_8} i_{\mathrm{dc}}dt = \frac{2T_1}{T_S}i_a + \frac{2T_2}{T_S}(i_a + i_c) = \frac{3MI_+\cos\phi}{4} - \frac{3MI_-}{4}\cos(2\omega t - \theta). \quad (16)$$

Similarly, the dc-link average currents over one carrier period in other five intervals B–F can be determined as

$$I_{\mathrm{dc}B} = I_{\mathrm{dc}C} = I_{\mathrm{dc}D} = I_{\mathrm{dc}E} = I_{\mathrm{dc}F} = \frac{3MI_+\cos\phi}{4} - \frac{3MI_-}{4}\cos(2\omega t - \theta). \quad (17)$$

It is noticed that the equations of the dc-link average currents over one carrier period in six intervals are the same. However, the right term of (17) is variable during different intervals because cos(2ωt–θ) varies with the time t. Obviously, when the load is balanced, the negative-sequence component I_- is zero. Consequently, the term of the second harmonic does not exist, and the dc-link average current is a constant, which is determined by the load and modulation index. It means that the dc-link current only contains of the dc current and high frequency harmonics around the switching frequency and its multiples. Nevertheless, when the load is unbalanced, I_- is not zero. Therefore, the dc-link harmonic current consists of not only high frequency harmonic currents but also the double fundamental frequency current. The peak value of the double fundamental frequency current is 3MI_-/4.

According to (16) and (17), the dc-link average current over one fundamental period can be written as

$$I_{\mathrm{dc}} = \frac{3MI_+\cos\phi}{4}. \quad (18)$$

From the aforementioned equation, it can be seen that the dc-link average current is in direct proportion to the modulation index, positive-sequence component, and power factor. Also, the dc-link average current is independent of the negative-sequence component. Equation (18) determines the active power sourced from the dc source. When the inverter has no load, ϕ is almost $-90°$ because of the existence of the output filter capacitor C. As a result, the dc-link average current is zero, and the absorbed active power from the dc source is zero, when neglecting the power loss in the inverter. However, high frequency harmonic currents still exist due to the high frequency switching activity.

B. DC-Link Harmonic RMS Current

To calculate the dc-link harmonic rms current, the mean square current over one carrier period must be first obtained. The mean square value of the dc-link current over one carrier period in the interval can be expressed as

$$I_{cA}^2 = \frac{1}{T_S}\int_{t_0}^{t_8} i_{\mathrm{dc}}^2 dt = \frac{2T_1}{T_S}i_a^2 + \frac{2T_2}{T_S}(i_a + i_c)^2. \quad (19)$$

Substituting (5) and (14) into (19), the following result is obtained:

$$I_{cA}^2 = \frac{\sqrt{3}}{2}M\left[I_+\sin(\omega t - \phi) + I_-\sin(\omega t - \theta)\right]^2\sin(\omega t - 30°) + \frac{\sqrt{3}}{2}M\Big[I_+\sin(\omega t - \phi - 120°) + I_-\sin(\omega t - \theta + 120°)\Big]^2\cos\omega t. \quad (20)$$

According to the aforementioned equation, the mean square value of the dc-link current over the interval A can be calculated as

$$I_{\mathrm{ms}A}^2 = \frac{3}{\pi}\int_{\pi_3}^{\pi/2} I_{cA}^2 d\omega t = \frac{3\sqrt{3}}{2\pi}M\Bigg\{\left(\frac{1}{2} + \frac{1}{3}\cos 2\phi\right)I_+^2 + \left(\frac{1}{2} - \frac{1}{24}\cos 2\theta - \frac{\sqrt{3}}{24}\sin 2\theta\right)I_-^2 + \left[\frac{1}{4}\cos(\theta - \phi) - \frac{\sqrt{3}}{4}\sin(\theta - \phi) + \frac{5}{12}\cos(\theta + \phi) - \frac{5\sqrt{3}}{12}\sin(\theta + \phi)\right]I_+I_-\Bigg\}. \quad (21)$$

Likewise, the mean square values of the dc-link current over other intervals B–F can be calculated as

$$I_{\mathrm{ms}B}^2 = \frac{3\sqrt{3}}{2\pi}M\Bigg\{\left(\frac{1}{2} + \frac{1}{3}\cos 2\phi\right)I_+^2 + \left(\frac{1}{2} - \frac{1}{24}\cos 2\theta + \frac{\sqrt{3}}{24}\sin 2\theta\right)I_-^2 + \left[\frac{1}{4}\cos(\theta - \phi) + \frac{\sqrt{3}}{4}\sin(\theta - \phi) + \frac{5}{12}\cos(\theta + \phi) + \frac{5\sqrt{3}}{12}\sin(\theta + \phi)\right]I_+I_-\Bigg\} \quad (22)$$

$$I_{\mathrm{ms}C}^2 = \frac{3\sqrt{3}}{2\pi}MI_+^2\left(\frac{1}{2} + \frac{1}{3}\cos 2\phi\right) + \frac{3\sqrt{3}}{2\pi}MI_-^2\left(\frac{1}{2} + \frac{1}{12}\cos 2\theta\right) - \frac{3\sqrt{3}}{2\pi}MI_+I_-\left[\frac{1}{2}\cos(\theta - \phi) + \frac{5}{6}\cos(\theta + \phi)\right] \quad (23)$$

$$I_{\mathrm{ms}D}^2 = \frac{3\sqrt{3}}{2\pi}M\Bigg\{\left(\frac{1}{2} + \frac{1}{3}\cos 2\phi\right)I_+^2 + \left(\frac{1}{2} - \frac{1}{24}\cos 2\theta - \frac{\sqrt{3}}{24}\sin 2\theta\right)I_-^2$$

$$+\left[\frac{1}{4}\cos(\theta-\phi)-\frac{\sqrt{3}}{4}\sin(\theta-\phi)+\frac{5}{12}\cos(\theta+\phi)-\frac{5\sqrt{3}}{12}\sin(\theta+\phi)\right]I_+I_-\Bigg\} \quad (24)$$

$$I_{\mathrm{ms}E}^2 = \frac{3\sqrt{3}}{2\pi}M\Bigg\{\left(\frac{1}{2}+\frac{1}{3}\cos 2\phi\right)I_+^2 + \left(\frac{1}{2}-\frac{1}{24}\cos 2\theta+\frac{\sqrt{3}}{24}\sin 2\theta\right)I_-^2 + \left[\frac{1}{4}\cos(\theta-\phi)+\frac{\sqrt{3}}{4}\sin(\theta-\phi)+\frac{5}{12}\cos(\theta+\phi)+\frac{5\sqrt{3}}{12}\sin(\theta+\phi)\right]I_+I_-\Bigg\} \quad (25)$$

$$I_{\mathrm{ms}F}^2 = \frac{3\sqrt{3}}{2\pi}MI_+^2\left(\frac{1}{2}+\frac{1}{3}\cos 2\phi\right) + \frac{3\sqrt{3}}{2\pi}MI_-^2\left(\frac{1}{2}+\frac{1}{12}\cos 2\theta\right) - \frac{3\sqrt{3}}{2\pi}MI_+I_-\left[\frac{1}{2}\cos(\theta-\phi)+\frac{5}{6}\cos(\theta+\phi)\right] \quad (26)$$

The dc-link mean square current over one fundamental period is the sum of the mean square values in six intervals A–F. Therefore, according to (21)–(26), the dc-link mean square current can be written as

$$I_{\mathrm{ms}}^2 = \frac{3\sqrt{3}}{2\pi}M\left(\frac{1}{2}I_+^2+\frac{1}{3}I_+^2\cos 2\phi+\frac{1}{2}I_-^2\right). \quad (27)$$

Finally, the dc-link harmonics rms current can be calculated as

$$\tilde{I}_{\mathrm{rms}} = \sqrt{I_{\mathrm{ms}}^2 - I_{\mathrm{dc}}^2} = \sqrt{M\left[\frac{\sqrt{3}}{4\pi}I_+^2+\left(\frac{\sqrt{3}}{\pi}-\frac{9}{16}M\right)I_+^2\cos^2\phi+\frac{3\sqrt{3}}{4\pi}I_-^2\right]}. \quad (28)$$

From the aforementioned equation, it can be seen that the dc-link harmonic rms current is determined by the modulation index, positive-sequence component, negative-sequence component, and power factor. The dc-link capacitor must endure the dc-link harmonic rms current. The dc-link harmonic rms current contains the double fundamental frequency harmonic and high frequency harmonics, and high frequency harmonic currents can be easily separated from the dc-link harmonic rms current because the peak value of the double fundamental frequency current is $3MI_-/4$.

V. DC-Link Voltage Ripple for Balanced and Unbalanced Load

To calculate the dc-link voltage ripple, the capacitor current i_C must be obtained. From the equivalent circuit in Fig. 2, the capacitor current can be written as

$$i_C = i_L - i_{\mathrm{dc}}. \quad (29)$$

The currents i_{dc}, i_C, and i_L can be divided into the average and harmonic components. The average component of i_C is zero because the impedance of the capacitor is infinity for the dc frequency. As a result, the average component of the dc-link current, I_{dc}, is equal to the average component of the input current, I_L. On the other hand, compared to the current ripple of i_{dc}, the current ripple of i_L is very small, if the dc-link capacitor is well designed. Therefore, the dc-link capacitor almost carries all harmonics of the dc-link current, including the double fundamental frequency harmonic. As a result, the dc-link capacitor voltage is expressed as

$$v_C = v_{C0}+\frac{1}{C_{\mathrm{dc}}}\int i_C\,dt = v_{C0}+\frac{1}{C_{\mathrm{dc}}}\int (I_{\mathrm{dc}}-i_{\mathrm{dc}})dt = v_{C0}+\Delta V_C \quad (30)$$

where v_{C0} is the initial value of v_C, and ΔV_C is the dc-link voltage ripple. From Fig. 4, it can be seen that the voltage ripple appears during four periods: $2T_0$, T_1+T_2 (t_1 to t_3), $2T_3$ (t_3 to t_5), and T_2+T_1 (t_5 to t_7) over one carrier period. Due to the symmetry, the voltage ripples during T_1+T_2 and T_2+T_1 are the same.

A. DC-Link Voltage Ripple under Balanced Load

Under the balanced load condition, I_- is zero. In this case, the dc-link average current over one carrier period in each interval is always constant, and the average value of the dc-link capacitor current over one carrier period is zero. It means that the initial and final values of the dc-link capacitor over one carrier period are the same. Therefore, the dc-link voltage ripple is determined by the voltage ripple during one carrier period. Taking the interval A as an example, the voltage ripple during $2T_0$ can be calculated as

$$\Delta V_{C1} = \frac{3MT_SI_+\cos\phi}{8C_{\mathrm{dc}}}\left[1-M\sin\omega t-Mv_z\right]. \quad (31)$$

The voltage ripples during T_1+T_2 or T_2+T_1 can be expressed as

$$\Delta V_{C2} = -\frac{3MT_SI_+\cos\phi}{16C_{\mathrm{dc}}}\left[2-M\sin\omega t+M\sin(\omega t-120^\circ)\right]. \quad (32)$$

The voltage ripple during $2T_3$ is given by

$$\Delta V_{C3} = \frac{3MT_SI_+\cos\phi}{8C_{\mathrm{dc}}}\left[1+M\sin(\omega t-120^\circ)+Mv_z\right]. \quad (33)$$

Because the inverter operation is symmetrical under the balanced load, the results in other five intervals are the same.

B. DC-Link Voltage Ripple Under Unbalanced Load

Under the unbalanced load condition, I_- is not equal to zero. Because the sum of i_a, i_b, and i_c is zero, the voltage ripple during $2T_0$ and $2T_3$ is the same as (31) and (33), respectively. The voltage ripples during $T_1 + T_2$ or $T_2 + T_1$ can be calculated as

$$\Delta V_{C4} = -\frac{3MT_S I_+ \cos\phi}{16C_{\rm dc}}[2 - M\sin\omega t + M\sin(\omega t - 120^\circ)] + \frac{3MI_-T_S}{8C_{\rm dc}}\cos(2\omega t - \theta). \quad (34)$$

According to (31), (33), and (34), the dc-link voltage ripple over one carrier period is expressed as

$$\Delta V_{CT} = \frac{3MI_-T_S}{4C_{\rm dc}}\cos(2\omega t - \theta). \quad (35)$$

Obviously, cos(2ωt–θ) is a double fundamental frequency sinusoid. Neglecting high-frequency voltage ripple, the dc-link voltage ripple is at double fundamental frequency, because the voltage ripple is the integral result over one fundamental period. In this case, the peak-to-peak value of the voltage ripple appears during a quarter of one fundamental period. The integral value of the dc-link voltage ripple during a quarter of one fundamental period can be obtained as

$$\Delta V_C = \int_{T\bullet\delta/2\pi}^{T\bullet\delta/2\pi+T/4} \frac{\Delta V_{CT}}{T_S}dt = \frac{3MI_-}{8\pi f C_{dc}}\sin(\theta - 2\delta) \quad (36)$$

where δ is the initial integral degree, f is the fundamental frequency, and T is the fundamental period. Because δ can vary randomly, the peak-to-peak value of the dc-link voltage ripple is

$$\Delta V_{C\rm pp} = \frac{3MI_-}{8\pi f C_{\rm dc}}. \quad (37)$$

When the unbalanced load exists, the value of (37) is far more than the values of (31), (33), and (34). It means that high frequency voltage ripple can be neglected and the double fundamental frequency harmonic dominates in the dc-link voltage ripple. Defining the dc-link voltage ripple as a half of $\Delta V_{C\rm pp}$, the dc-link capacitor can be written as

$$C_{\rm dc} = \frac{3MI_-}{16\pi f \Delta V_C}. \quad (38)$$

From the aforementioned equation, it can be found that the dc-link capacitor is in inverse proportion to the dc-link voltage ripple. It means that the larger the dc-link capacitance is, the smaller the dc-link voltage ripple is, and vice versa. Therefore, a tradeoff must be made between the dc-link voltage ripple and volume. Moreover, the dc-link voltage capacitor is in direct proportion to the modulation index. Due to the variability of the modulation index, the maximum modulation index is used to design the dc-link capacitor. In general, the dc-link voltage ripple should be smaller than the 10% dc voltage to ensure that the output voltages are sinusoidal. Finally, the designed capacitance should be larger than the calculated one based on (38).

TABLE I
ELEMENT PARAMETERS

T_1–T_6	FF800R12KE3
$L_{\rm dc}$	0.5 mH
$C_{\rm dc}$	2400 μF/600 V
L	112 μH
C	1200 μF
K	1:1.07

TABLE II
SOME PARAMETERS FOR CALCULATION

Load conditions	Balanced load	Phase a with half load	Phase a and b with half load
I_+	244.22 A	199.3 A	155.12 A
I_-	0 A	46.15 A	46.15 A
cosϕ	0.907	0.92614	0.95197

Once again, it should be noted that the dc-link capacitor must endure the dc-link harmonic rms current, aside from the requirement of the dc-link voltage ripple.

VI. EXPERIMENTAL RESULTS

In order to verify the accuracy of the proposed calculating method, a three-phase bridge inverter prototype has been implemented. The imbalance is defined in Section III, and the percentage of the unbalanced load is 50%. The inverter is designed to have the rated output voltages and currents of 380 V and 105 A at 360–520 V dc input (the modulation index is from 1 to 0.69). The three-phase inductive load is connected to the inverter in the star formation, and the paralleled load resistor and inductor are 2.62 Ω and 11.1 mH, respectively. The output frequency is 50 Hz, and the switching frequency is 5.4 kHz. *K* is the turn ratio of the primary and secondary windings. The TI DSP TMS320F28335 is used as the controller of the inverter. Based on the theoretical analysis, the maximum harmonics rms current and dc-link capacitance are calculated as 110 A and 1326 μF. Finally, the dc-link capacitor is chosen as 4600 μF/600 V film capacitors connected in parallel. Some other inverter parameters are shown in Table I.

In the experimental setup, the dc-link current and voltage are measured by high bandwidth current probe and high voltage probe. The data are saved in the oscilloscope and exported to the computer, because the oscilloscope cannot calculate the harmonic rms current. Therefore, based on the measured data, the experimental average and harmonic rms currents are obtained by using the FFT analysis in the MATLAB software. On the other hand, the calculation results of the dc-link current and voltage are obtained according to (18), (28), and (37). Some parameters for the calculation under the different load conditions, including I_+, I_-, and cosϕ, are shown in Table II. It can be noticed that the negative-sequence peak currents are identical under the unbalanced load conditions.

Figs. 8–10 compare the experimental and calculated results of the dc-link average and harmonic rms currents as a function

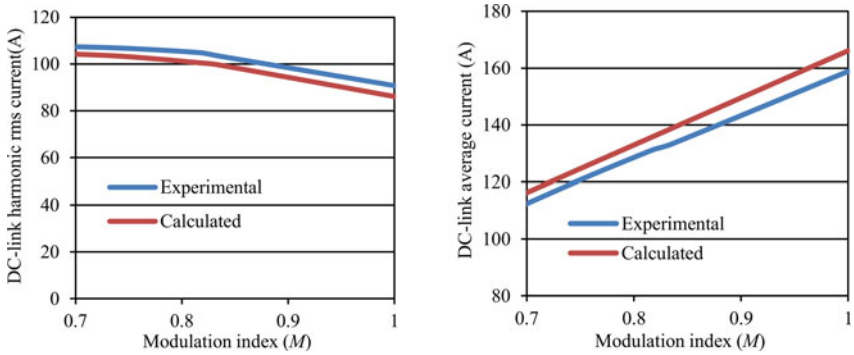

Fig. 8. Experimental and calculated comparison results with balanced load.

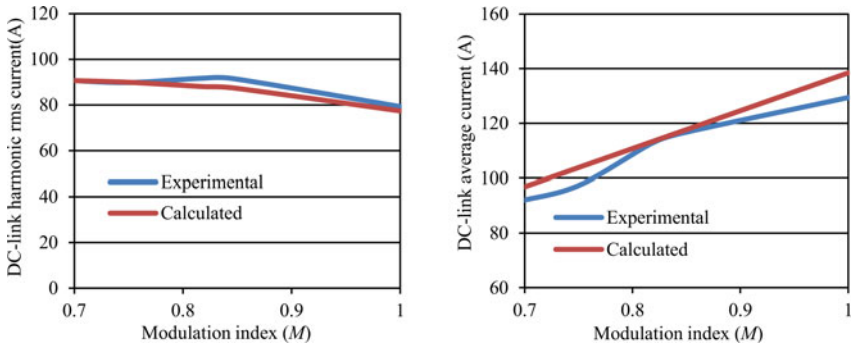

Fig. 9. Experimental and calculated comparison results when phase *a* with half load.

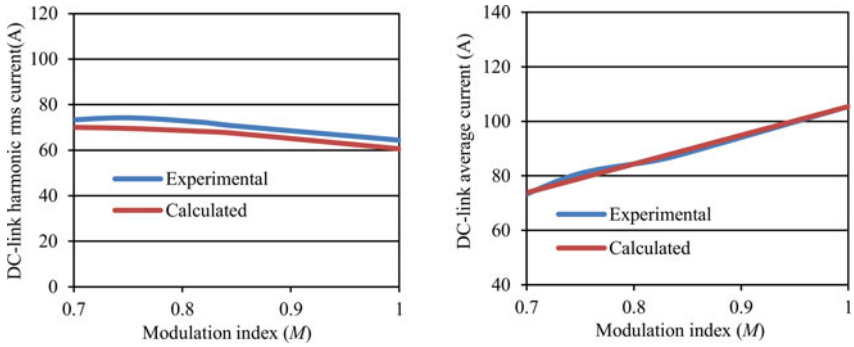

Fig. 10. Experimental and calculated comparison results when phases *a* and *b* with half load.

of the modulation index with the balanced load, phase *a* with the half load, and phases *a* and *b* with the half load. It can be found that a good agreement between the calculated and experimental results is achieved. Moreover, it is shown that the dc-link harmonic rms current decreases with the increase of the modulation index, and however, the dc-link average current is directly proportional to the modulation index. In addition, it can also be found that the dc-link harmonic rms and average currents reduce with the drop of the output power.

Fig. 11 illustrates the experimental result of the dc-link voltage ripple at 400-V dc input under the balanced load. It is shown that the voltage ripple is less than 3 V, as expected in (31)–(33), when neglecting the voltage spike. The voltage spike appears at the switching instant due to the parasitic inductance and is out of scope of this paper. The experimental results at other input voltages are the same as Fig. 11, and are not shown here.

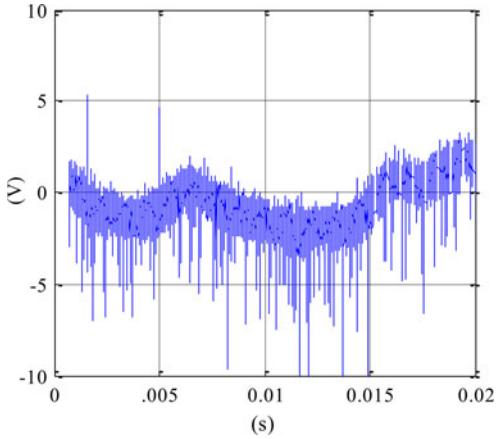

Fig. 11. Experimental result of the dc-link voltage ripple under the balanced load.

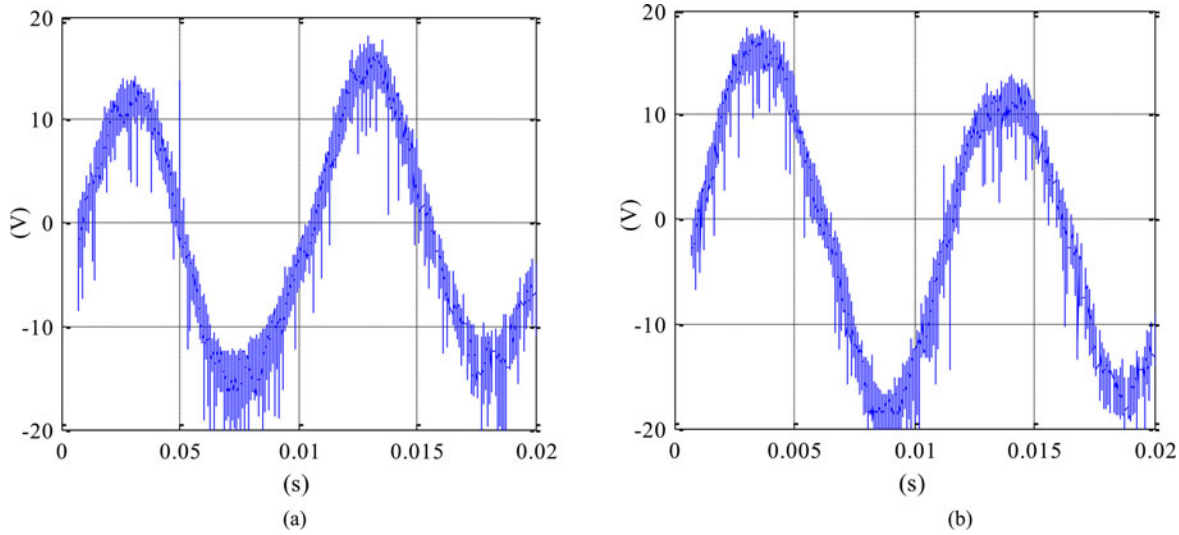

Fig. 12. Experimental results of the dc-link voltage ripple under the unbalanced loads (a) Experimental voltage ripple when phase *a* with half load (b) Experimental voltage ripple when phase *a* and *b* with half load.

TABLE III
EXPERIMENTAL AND CALCULATED RESULTS OF DC-LINK VOLTAGE RIPPLES

Modulation index (*M*)	Experimental voltage ripple when Phase *a* with half load	Experimental voltage ripple when Phases *a* and *b* with half load	Calculated voltage ripple
1.0 (360V)	20.5 V	22.5 V	23.2 V
0.9 (400V)	18.5 V	20.5 V	20.7 V
0.82 (440V)	17 V	18 V	18.9 V
0.75 (480V)	14.5 V	16 V	17.2 V
0.69 (520V)	13.5 V	15 V	15.9 V

Fig. 12(a) and (b) show the experimental results of the dc-link voltage ripple at 400-V dc input, when phase *a* carries the half load and phases *a* and *b* carry the half load, respectively. It can be seen that the dc-link voltage ripple is at double fundamental frequency and the peak-to-peak value of the dc-link voltage ripples are approximately 18.5 and 20.5 V, compared to the calculated value 20.7 V. In comparison with the voltage ripple under the balanced load, it is much larger. Moreover, it can be noticed that the dc-link voltage ripples under both conditions are almost identical, because both the peak currents of the negative sequence are 46.15 A. Therefore, for the same dc input, the dc-link voltage ripples are basically equivalent, as illustrated in Table III. Other experimental waveforms under the conditions in Table III are not presented here, since they are similar to Fig. 12.

VII. CONCLUSION

This paper puts forward the analysis and calculation of the dc-link current and voltage ripples for the three-phase inverter with the unbalanced load. It is shown that high frequency harmonics of the output currents can be omitted through the caparison of the dc-link average and rms currents between the balanced and unbalanced loads. The dc-link average and harmonic rms currents are derived, and the dc-link voltage ripple is obtained. It is found that the current and voltage ripples consist of the double fundamental frequency harmonic, apart from high frequency harmonics. Experimental results validate the accuracy of the theoretical calculation. The calculated result can be used to guide the dc-link capacitor design.

APPENDIX

Assuming i_{la}, i_{lb}, and i_{lc} are the load currents of phases *a*, *b*, and *c*, respectively. Therefore, ignoring the magnetizing currents, the currents of the primary windings are given by

$$\begin{cases} i_{Pa} = i_{la}/K \\ i_{Pb} = i_{lb}/K \\ i_{Pc} = i_{lc}/K. \end{cases} \tag{A-1}$$

The input currents of the transformer can be expressed as

$$\begin{cases} i_{oa} = i_{Pa} - i_{Pc} \\ i_{ob} = i_{Pb} - i_{Pa} \\ i_{oc} = i_{Pc} - i_{Pb}. \end{cases} \tag{A-2}$$

Therefore, the output currents of the inverter bridge can be written as

$$\begin{cases} i_a = i_{Ca} + \dfrac{i_{la} - i_{lc}}{K} \\ i_b = i_{Cb} + \dfrac{i_{lb} - i_{la}}{K} \\ i_c = i_{Cc} + \dfrac{i_{lc} - i_{lb}}{K} \end{cases} \tag{A-3}$$

where i_{Ca}, i_{Cb}, and i_{Cc} are the filter capacitor currents of phases *a*, *b*, and *c*, respectively.

According to (A.3), three currents $I_{\rm a}$, $I_{\rm b}$, and $I_{\rm c}$ can be obtained. Therefore, the positive- and negative-sequence components can be correspondingly obtained based on the

transformation equation (13). As a result, I_+ and I_-, and ϕ and θ can be calculated.

REFERENCES

[1] J. Salmon, A. M. Knight, and J. Ewanchuk, "Single-phase multilevel PWM inverter topologies using coupled inductors," *IEEE Trans. Power Electron.*, vol. 24, no. 5, pp. 1259–1266, May 2009.

[2] O. Dordevic, E. Levi, and M. Jones, "A vector space decomposition based space vector PWM algorithm for a three-level seven-phase voltage source inverter," *IEEE Trans. Power Electron.*, vol. 28, no. 2, pp. 637–649, Feb. 2013.

[3] Y. S. Lai, Y. K. Lin, and C. W. Chen, "New hybrid pulsewidth modulation technique to reduce current distortion and extend current reconstruction range for a three-phase inverterusing only DC-link sensor," *IEEE Trans. Power Electron*., vol. 28, no. 3, pp. 1331–1337, Mar. 2013.

[4] S. Das, G. Narayanan, and M. Pandey, "Space-vector-based hybrid pulsewidth modulationtechniques for a three-level inverter," *IEEE Trans. Power Electron.*, vol. 29, no. 9, pp. 4580–4591, Sep. 2014.

[5] D. G. Holmes and T. A. Lipo, *Pulse Width Modulation for Power Converters*. Piscataway, NJ, USA: IEEE Press, 2003.

[6] X. Pei and Y. Kang, "Short-circuit fault protection strategy for high power three-phase three-wire inverter," *IEEE Trans. Ind. Informat.*, vol. 8, no. 3, pp. 545–553, Aug. 2012.

[7] J. S. Lai, H. Kouns, and J. Bond, "A low-inductance DC bus capacitor for high power traction motor drive inverters," in *Proc. IEEE Ind. Appl. Conf.*, pp. 955–962, 2002.

[8] G. Chen, R. Burgos, Z. Liang, F. Lacaux, F. Wang, J. D. van Wyk, W. G. Odendaal, and D. Boroyevich, "Reliability-oriented design considerations for high-power converter modules," in *Proc. IEEE Power Electron. Spec. Conf.*, vol. 1, pp. 419–425, 2004.

[9] A. M. Hava, U. Ayhan, and V. V. Aban, "A DC bus capacitor design method for various inverter applications," in *Proc. IEEE Energy Convers. Congr. Expo.*, pp. 4592–4599, 2012.

[10] H. Wen, W. Xiao, X. Wen, and P. Armstrong, "Analysis and evaluation of DC-Link capacitors for high-power-density electric vehicle drive systems," *IEEE Trans. Veh. Technol.*, vol. 61, no. 7, pp. 2950–2964, Sep. 2012.

[11] A. Mariscotti, "Analysis of the DC-link current spectrum in voltage source inverters," *IEEE Trans. Circuits Syst. I, Reg. Papers*, vol. 49, no. 4, pp. 484–491, Sep. 2002.

[12] B. P. Mcgrath and D. G. Holmes, "A general analytical method for calculating inverter DC-link current harmonics," *IEEE Trans. Ind. Appl.*, vol. 45, no. 5, pp. 1851–1859, Sep. 2009.

[13] U. Ayhan and A. M. Hava, "Analysis and characterization of DC Bus ripple current of two-level inverters using the equivalent centered harmonic approach," in *Proc. IEEE Energy Convers. Congr. Expo.*, pp. 3830–3837, 2011.

[14] M. H. Bierhoff and F. W. Fuchs, "DC-link harmonics of three-phase voltage-source converters influenced by the pulse-width-modulation strategy—An analysis," *IEEE Trans. Ind. Electron.*, vol. 55, no. 5, pp. 2085–2092, May 2008.

[15] F. Renken, "The DC-link capacitor current in pulsed single-phase H-bridge inverters," in *Proc. Eur. Conf. Power Electron.*, 2005 pp. 1–10.

[16] P. A. Dahono, Y. Sato, and T. Kataoka, "Analysis and minimization of ripple components of input current and voltage of PWM inverters," *IEEE Trans. Ind. Appl.*, vol. 32, no. 4, pp. 945–950, Jul. 1996.

[17] J. W. Kolar and S. D. Round, "Analytical calculation of the RMS current stress on the DC-link capacitor of voltage-PWM converter systems," *Proc. IEE*, vol. 153, no. 4, pp. 535–543, Jul. 2006.

[18] J. Hobraiche, J. Vilain, P. Macret, and N. Patin, "A new PWM strategy to reduce the inverter input current ripples," *IEEE Trans. Power Electron.*, vol. 24, no. 1, pp. 172–180, Jan. 2009.

[19] A. M. Cross, P. D. Evans, and A. J. Forsyth, "DC link current in PWM inverters with unbalanced and non-linear loads," *Proc. IEE*, vol. 146, no. 6, pp. 620–626, Nov. 1999.

[20] *Military Standard - Aircraft Electric Power Characteristic*, MIL-STD-704E, 1991.

Xuejun Pei (M'12) received the B.E., M.E., and Ph.D. degrees in electrical engineering from the Huazhong University of Science and Technology, Wuhan, China, in 1998, 2001, and 2004, respectively.

In 2004, he joined the Huazhong University of Science and Technology as a Teaching Assistant, where since 2006, he has been an Associate Professor with the College of Electrical and Electronic Engineering. From March 2011 to March 2012, he was a Visiting Scholar at Michigan State University, East Lansing, USA. His research interests include high-power converter, EMC issue, fault diagnosis of power electronics, and the related control techniques.

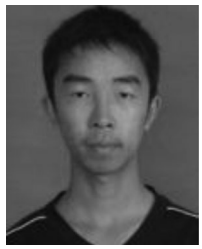

Wu Zhou was born in Hubei, China, on August 10, 1990. He received the B.E. degree in electrical and electronic engineering from the Huazhong University of Science and Technology, Wuhan, China, in 2012, where he is currently working toward the Ph.D. degree.

His research interests include high-power drive system and EMI.

Yong Kang received the B.E., M.E, and Ph.D. degrees from the Huazhong University of Science and Technology, Wuhan, China, in 1988, 1991, and 1994, respectively.

In 1994, he joined the Huazhong University of Science and Technology as a Lecturer and was promoted to an Associate professor in 1996 and to a Full Professor in 1998. He is currently the Head of the College of Electrical and Electronic Engineering, Huazhong University of Science and Technology. He is the author of more than 60 technical papers. His research interests include power electronic converter, ac drivers, electromagnetic compatibility, and their digital control techniques.